# Cyclic behavior of very short steel shear links

Xiaodong Ji[1], Yandong Wang[2], Qifeng Ma[3], and Taichiro Okazaki[4]

*[1] Associate professor, Key Laboratory of Civil Engineering Safety and Durability of China Education Ministry, Department of Civil Engineering, Tsinghua University, Beijing 100084, China*

*[2] Graduate student, Department of Civil Engineering, Tsinghua University, Beijing 100084, China*

*[3] Graduate student, Department of Civil Engineering, Tsinghua University, Beijing 100084, China*

*[4] Associate professor, Graduate School of Engineering, Hokkaido University, Sapporo, Hokkaido 060-8628, Japan*

**Abstract:** A replaceable coupling beam is proposed which comprises steel hybrid shear links that are shorter than typical shear links in eccentrically braced frames (EBFs). Cyclic loading tests were conducted to examine the behavior of these very short shear links. The test variables included the steel type, length ratio, web stiffener configuration, and loading protocol. The link specimens showed two types of failure modes: link web fracture and fracture at the weld connecting link flange to end plate. The link specimens had an inelastic rotation capacity of approximately 0.14 rad, which is significantly larger than the capacity assumed for EBF links. Links using LY225 steel instead of Q235 steel achieved a 25% increase in inelastic rotation and 44% increase in cumulative plastic rotation. The overstrength factors of the very short shear links reached 1.9, significantly exceeding 1.5 which is the value assumed for EBF links

Please cite this article as: Xiaodong Ji, Yandong Wang, Qifeng Ma, Taichiro Okazaki. Cyclic behavior of very short steel shear links. Journal of Structural Engineering, 2016, 142(2): 04015114.
doi: 10.1061/(ASCE)ST.1943-541X.0001375

by design provisions. Analysis suggests that large overstrength can develop in very short shear links due to the contribution of flanges and cyclic hardening of web steel under large plastic strains. Axial deformation was measured as the links underwent inelastic shear deformation. The extent of axial deformation might be explained by simple plasticity theory.

**Keywords**: shear link; replaceable coupling beam; seismic behavior; overstrength; inelastic rotation; axial deformation

## Introduction

Reinforced concrete (RC) coupled-wall systems where RC coupling beams connect two or more wall piers in series are frequently used in high-rise buildings. When this structural system is subjected to severe ground motion, the RC coupling beams dissipate seismic energy as they undergo large inelastic deformation. However, without special reinforcing, RC coupling beams are prone to non-ductile failure. In addition, post-damage repair of RC coupling beams is costly in both expense and time. In recent years, steel coupling beams have been recognized as an alternative to RC coupling beams. The ends of the steel coupling beams are embedded in the boundary elements of the RC wall piers, and the resulting structural system is referred to as a hybrid coupled-wall system (El-Tawil et al. 2010). The steel coupling beams provide very stable hysteretic behavior by yielding in shear and offer excellent ductility under cyclic loading. Nevertheless, post-damage repair of the steel coupling beams is still costly because replacement of the entire beam is unfeasible.

To overcome this difficulty, Fortney et al. (2007) proposed the concept of replaceable steel coupling beams, where a “fuse” shear link is incorporated within the beam. Fig.1 shows a schematic view of the replaceable steel coupling beam which comprises a central “fuse” shear link connected to permanent steel segments at its two ends. Inelastic deformation is expected to concentrate in the “fuse” shear links during a severe earthquake, and seismic energy is dissipated by these links distributed over the height of the coupled wall. The shear link can be replaced readily after being damaged because specialized connections are employed at its two ends, thus improving the resiliency of building structures against seismic hazards. Lately, Chung et al. (2009) and Christopoulos et al. (2013) extend this concept by using friction dampers or viscous dampers as the “fuse” elements.

Extensive data (Hjelmstad and Popov 1983; Malley and Popov 1984, Kasai and Popov 1986; Popov and Engelhardt 1988; Engelhardt and Popov 1989; Okazaki et al. 2005; Okazaki and Engelhardt 2007) indicates that a properly detailed shear link can provide stable, ductile and predictable behavior under cyclic loading. Note that these tests targeted the links used for eccentrically braced frames (EBFs) and they mostly had a length ratio, $e/(M_p/V_p)$, of over 1.0, where $e$ denotes the link length, and $M_p$ and $V_p$ denotes the plastic flexural strength and shear strength of the link, respectively. However, the short span of coupling beams and the necessity to limit the fuse weight for replacement requires the use of very short shear links for coupling beams. These very short shear links commonly have a length ratio smaller than 1.0. Such short links can develop a significantly higher overstrength than common EBF links, as indicated in McDaniel et al. (2003) and Dusicka et al. (2010). In addition, hybrid sections with low-yield-strength steel in the web might be used to promote early yielding and increase the inelastic rotation capacity. Therefore, there is a clear need to investigate the cyclic loading behavior of very short shear links made of low-yield-strength steel.

The next section of this paper describes an experimental program where twelve shear links were subjected to cyclic loading. The third section presents the test results and discusses the hysteretic responses, failure mode, and strength and deformation capacities. Finally, the fourth section analyzes the overstrength factor for very short shear links.

## Experimental program

### *Test specimens*

The test specimens represented the shear links used in the replaceable steel coupling beams for the core-wall of a 130-m tall building (Ji et al. 2014). To accommodate the capacity of the loading facility, the specimens were fabricated at 3/5 scale in geometric dimension. A total of twelve link specimens were considered in the test. Fig. 2 shows the geometry and details of the specimens. The shear links were built-up I-shapes with a depth, width, web thickness, and flange thickness of 400, 180, 10, and 14 mm, respectively. The width-to-thickness ratio of the flanges was 6.4 and the depth-to-thickness ratio of the web was 37.2. Both the link flange and web satisfied the requirement for highly ductile members by the AISC 341-10 provisions.

The flanges and web were welded together by complete-joint-penetration (CJP) groove welds. The stiffeners were full depth, welded to the web and to both flanges using fillet welds. The shear link was welded to heavy end plates at each end by CJP groove welds. All the welds were performed by the flux-cored-arc welding process with E50 electrodes. The welds were qualified by both ultrasonic testing and magnetic particle testing. Charpy V-notch (CVN) toughness of the welds averaged over three specimens was 170.6 J at 21 ℃ and 111.1 J at

-29 ℃. To delay the web fracture at the region where the flange-to-web CJP groove weld and the fillet welds of the stiffeners meet, the vertical fillet welds of the web stiffeners were terminated at a distance of five times the web thickness from the toe of the flange-to-web weld per the suggestion by Okazaki et al. (2005) and Okazaki and Engelhardt (2007).

The shear link specimens adopted hybrid sections. The flanges were made of Q345 steel (nominal yield strength $f_y$ = 345 MPa), and the stiffeners of Q235 steel ($f_y$ = 235 MPa). The webs for the specimens with “L” in the nomenclature were made of low-yield-strength steel LY225 ($f_y$ = 225 MPa), while those for the specimens with “Q” in the nomenclature were made of Q235 steel. The measured material properties of steel by tensile coupon tests are summarized in Table 1. Note that the yield and ultimate strength listed in this table are the average values measured from three coupon tests. The measured yield strength of LY225 steel was 18% lower than that of Q235 steel, while its elongation was 23% higher than that of Q235 steel.

***Test variable***

In addition to the type of steel used for the web, the following variables were considered for the test: (1) link length ratio, (2) stiffener configuration, and (3) loading protocol. Table 2 summarizes the test variables for all specimens.

*Link length ratio*

The length of shear link specimens was 660 and 440mm, which corresponded to a length ratio $e/(M_p/V_p)$ of approximately 0.9 and 0.6, respectively. All link specimens had a length ratio smaller than 1.6 and, therefore, they were expected to yield primarily in shear per the AISC

341-10 provisions.

*Stiffener configuration*

The AISC 341-10 provisions require intermediate web stiffeners of shear links to be spaced at intervals not exceeding ($30t_w-d/5$), where $t_w$ denotes the web thickness and $d$ denotes the link depth. Most specimens were provided with intermediate web stiffeners spaced at 220mm, which is exactly at this limit. However, increase of stiffener spacing might be permissible if the web has a small width-to-thickness ratio as enabled by using low-yield-strength steel (Dusicka et al. 2010). Therefore, the stiffeners for Specimens L13 and Q13 (see Fig.2(c)) were intentionally designed with a larger spacing of $1.5\,(30t_w-d/5)$=330mm. In addition, Specimens L12 & Q12 and L22 & Q22 (see Fig. 2(b) and 2(e), respectively), were designed with stiffeners on one side of the web only. Other specimens had stiffeners on both sides of the web. Note that the AISC 341-10 provisions allow shear links with a depth less than 635 mm to use stiffeners on one side of the web only.

*Loading protocol*

Cyclic loading of the link specimens was controlled by the link rotation angle. For most specimens, the loading protocol specified by the AISC 341-10 provisions for testing EBF link-to-column connections, shown in Fig. 3(a), was used. Two other loading protocols were used for comparison. The first was the loading protocol for testing structural components specified by the Chinese specification of testing methods for earthquake resistant building (JGJ 101-96), shown in Fig. 3(b). The second was the loading protocol for testing low-cycle fatigue behavior of steel dampers specified by the Chinese specification for seismic energy dissipation of buildings (JGJ 297-2013), shown in Fig. 3(c). To investigate the influence of various loading protocols, two duplicates of Specimen L11, i.e., Specimens L11C and L11D, were fabricated. Specimen L11C was loaded with the JGJ 101-96 loading protocol, and Specimen L11D with the JGJ 297-2013 loading protocol.

### *Test setup and instrumentation*

Fig. 4 shows the test setup. The end plates of the shear link were bolted into the setup, between the loading beam and foundation beam. The pantograph system ensured that two ends of the shear link remained parallel to each other during testing. The centroid of the actuator passed through the mid-span of the link, ensuring the link would develop equal and opposite bending moments at the two ends. Out-of-plane support frames were provided to prevent out-of-plane deformation and twisting of the link during testing. The loading beam was vertically supported by a counterweight to allow no axial load in the link. The test was terminated when the specimen significantly lost its shear strength due to progress of fracture.

An instrumentation scheme was used to measure the shear load, displacement and strains of the specimens. Fig. 4 also shows the locations of linear variable differential transformers (LVDTs) and strain gauges placed on the specimen. A total of six LVDTs were used to measure the deformation of the specimen. Strain gauges were used to monitor the shear strains developed in the link web and the flanges at the link ends.

## Experimental results

### *Hysteretic responses*

All link specimens yielded in shear. Fig. 5 shows the hysteretic responses of shear force versus inelastic rotation relationship of the specimens. The inelastic rotation was evaluated by removing the elastic rotation, based on the response during early elastic cycles, from the total rotation of the link. The specimens that were exactly at the stiffener spacing limit showed very stable hysteretic loops even under inelastic rotation cycles exceeding 0.08 rad. However, Specimens L13 and Q13 exhibited a drop followed by recovery in strength after reaching an inelastic rotation of 0.10 rad (see Fig. 5(e) and 5(j)), which was associated with web buckling and subsequent development of a tension field during each load reversal.

Two values of the plastic shear strength are indicated in Fig. 5. The nominal value of plastic strength ($V_{pn}$) was calculated as $0.6f_yA_w$ per the AISC 341-10 provisions, using the nominal yield strength of the steel and nominal dimensions, while the measured value of plastic strength ($V_p$) was based on the actual measured yield strength of the steel and actual measured dimensions. It is notable that these two values are nearly identical for the LY225 web link. However, the value of $V_p$ was 13% higher than $V_{pn}$ for the Q235 web link due to the difference between nominal and measured yield strength of the Q235 steel.

***Failure mode***

After the link specimens yielded in shear, four types of damage were observed during testing: i) web buckling, ii) stiffener-to-flange weld fracture, iii) web fracture, and iv) flange-to-end plate weld fracture. Fig. 6 shows photographs of each damage type. Table 3 summarizes the progress of visually identified damage and the cause of ultimate failure. In this paper, failure of links is defined as the point where the link strength drops to below the plastic strength $V_p$, and the inelastic rotation capacity is taken as the maximum level of inelastic rotation sustained for at least one full cycle of loading prior to failure of the link.

It is notable that web buckling occurred earlier and developed faster in Specimens L13 and Q13 compared to the specimens which were exactly at the stiffener spacing limit. In the end, the development of the damage types iii) and iv) caused failure of the specimens. The web fracture initiated at the termination of a fillet weld connecting a stiffener to the web, which was likely induced by the high triaxial constraints that develop at the weld ends coupled with elevated local strain demands in this region (Chao et al. 2006). This observation is consistent with the past tests in McDaniel et al. (2003) and Okazaki et al. (2005; 2007). The fracture then propagated along the stiffener-to-web weld, and finally tore the web apart, as shown in Fig. 6(c). Fig. 6(d) shows a photograph of flange-to-end plate weld fracture, which was likely caused by low-cycle fatigue of tensile and compressive strains coupled with local bending of the flange. Comparing the three identical Specimens L11, L11C and L11D, web fracture and stiffener-to-flange fracture was observed in Specimens L11 and L11C, but not in Specimen 11D. This was perhaps because the inelastic rotation imposed in Specimen 11D was smaller than the other two.

***Shear strength***

Table 4 lists the measured value of plastic shear strength $V_p$ and maximum shear strength $V_{max}$ of the specimens. The overstrength factor of the shear link, $\Omega$, is defined as the ratio $V_{max}$ / $V_p$. The specimens with a length ratio of 0.6 developed a higher overstrength than those with a length ratio of 0.9. However, very small difference in overstrength factor was observed between specimens with LY225 and Q235 steel web. The specimens with stiffeners on one side of the web were found to have nearly identical overstrength as the counterpart specimens that used stiffeners on both sides. The average overstrength of the specimens that were exactly at the stiffener spacing limit was 1.9, which is larger than the value of 1.5 specified for EBF links in AISC 341-10. The overstrength of Specimens L13 and Q13 was approximately 1.65, which is 13% smaller than the specimens that were exactly at the stiffener spacing limit. In the two specimens, early development and progression of web buckling counteracted strain hardening effects. The overstrength will be examined further in Section 4.

***Deformation capacity***

The inelastic rotation capacity of the link specimens is listed in Table 4. The link specimens developed an inelastic rotation capacity of 0.14 rad on average, which was significantly larger than the value of 0.08 rad required in the AISC 341-10 provisions. The inelastic rotation of the LY225 web links was, on average, 25% larger than that of the Q235 web links. The difference between using single-side stiffeners or both-side stiffeners had very limited influence on the inelastic rotation capacity of the link specimens. Note that the reason why Specimen L11D achieved a much smaller inelastic rotation than the other links was because the JGJ 297-2013 loading protocol does not impose link rotation larger than 0.08 rad.

Table 4 also lists the cumulative plastic rotation ($\sum\gamma_p$) of the specimens. The difference in web steel type significantly affected the cumulative plastic rotation of the shear links. The LY 225 web links developed a cumulative plastic rotation of 3.35 rad on average, which was 44% larger than the value of 2.33 rad developed by the Q235 web links. However, the stiffener configuration caused limited influence on the cumulative plastic rotation of the shear links.

***Axial deformation***

LVDTs 5# and 6# measured the vertical displacement of the link specimens. The vertical displacement of the link specimens was small but not negligible. As stated earlier, the test setup ensured that no vertical force was applied to the specimens. Fig. 7(a) shows the measured displacement orbits of the top end plate relative to the bottom end plate for Specimen L11C. Other specimens showed similar response. At large deformation, the applied lateral load can be decomposed into two components, one perpendicular to the inclined link axis and another parallel to the link axis (see Fig. 7(b)). Similarly, the deformation of shear link can be decomposed into two components (see Fig. 7(c)). The first is the geometric deformation associated with link rotation, which recovers to zero at zero rotation. The second component is the axial deformation induced by the force parallel to the link axis. Fig. 7(d) illustrates how the link elongates during each inelastic loading cycle. The axial elongation increases with link rotation amplitude and accumulates with each half loading cycle.

***Discussions of deformations***

Fig. 8 shows the inelastic rotation collected from tests on steel links of various length ratios (Hjelmstad and Popov 1983; Malley and Popov 1984; Kasai and Popov 1986; Ricles and Popov 1986; Engelhardt and Popov 1989; McDaniel et al. 2003; Okazaki and Engelhardt 2007; Okazaki et al. 2009; Dusicka et al. 2010; Mansour et al. 2011). The inelastic rotation generally exceeded the AISC 341-10 requirement for link rotation capacity. The data that does not meet the AISC 341-10 requirement was tested under an overly severe loading protocol that imposed a large number of inelastic cycles at smaller rotation angles (Okazaki et al. 2005; Okazaki and Engelhardt 2007). Interestingly, the inelastic rotation obtained for very short shear links from this project exceeded the AISC requirement by a very large margin. McDaniel et al. (2003) and Dusicka et al. (2010) also tested shear links with a length ratio less than 1.0. The links in McDaniel et al. (2003) developed a low value of inelastic rotation smaller than the required 0.08 rad due to early brittle fracture of link web. They attribute the cause of early fracture to the termination of stiffener-to-web fillet weld being too close to the web-to-flange weld, which led to significant concentration of stress and plastic strain in the web-flange-stiffener intersection. The link specimens in Dusicka et al. (2010) included two types. The links designed without stiffeners using low-yield-strength steel reached an inelastic rotation of 0.20 rad by avoiding fracture at stiffener welds, while the conventional links failed at 0.12 rad inelastic rotation due to fracture along stiffener-to-web welds.

There is limited data for the axial deformations of shear links. However, this test indicates that the axial deformations develop as the shear links undergo large inelastic rotation. If the axial deformation is restrained by the adjacent wall piers, non-negligible axial forces can develop in replaceable coupling beams (Teshigawara et al., 1998). In fact, a high level of axial force was observed in recent tests on large-scale replaceable steel coupling beams by the writers, which will be discussed in a future paper. The axial force may affect the behavior of shear links, concrete slabs above coupling beams and the joints between coupling beams and wall piers. Therefore, the effect of axial forces should be accounted for when using very short shear links in coupling beams.

## Analysis of overstrength

The overstrength factor of a shear link is an important parameter for capacity design of its adjacent elements and connections. As presented previously, the measured overstrength factor of the very short link specimens was 1.9 on average, much greater than the value of 1.5 assumed for EBF links in the AISC 341-10 provisions. The substantially larger overstrength was examined by collection of test data and finite element (FE) analysis.

### *Data collection of overstrength factors*

Fig. 9 summarizes data from 111 link tests (Hjelmstad and Popov 1983; Malley and Popov 1984; Kasai and Popov 1986; Ricles and Popov 1986; Engelhardt and Popov 1989; Ramadan and Ghobarah 1995; McDaniel et al. 2003; Okazaki and Engelhardt 2007; Okazaki et al. 2009; Dusicka et al. 2010; Mansour et al. 2011) and from this program, plotting the ratio $V_{max}/V_n$ against the link length ratio in the range of 0.47 to 4.37. $V_n$ is the inelastic strength of the link, and was calculated as the smaller of $V_p$ or $2M_p/e$, where $V_p$ and $M_p$ were computed using the actual measured dimensions and actual measured yield strengths of steel. The overstrength factor of 1.5, suggested by Popov and Engelhardt (1988), is somewhat conservative for shear links with a length ratio of over 1.0. However, the shear links with a length ratio smaller than 1.0 can develop overstrength factors significantly larger than 1.5. Similar findings are obtained in recent tests by McDaniel et al. (2003) and Dusicka et al. (2010). The tests indicate that the overstrength of very short links with built-up section is close to 2.0.

### *Reasons for large value of overstrength*

It was suspected that the substantially larger overstrength in very short shear links was caused by two causes. The first cause is the shear resistance of flanges (Itani 2002; Richards 2004). The second is the cyclic hardening effect of web steel under large inelastic strains (Kasai et al. 2004). Finite element analysis was used to quantify the contribution of the two causes to the overstrength.

*Finite element model*

A number of finite element models were developed using the program Abaqus 6.10 (2009). The link model was discretized using 20-node second-order reduced integration solid elements. Mesh sensitivity studies showed that convergence of the model is achieved by using two elements across the thickness of flanges, web, stiffeners and end plates. As in the test setup, one end plate was completely fixed, while the other end plate was restrained from out-of-plane motion or rotation about any three axes, and free to translate in the axial and perpendicular directions. Both material nonlinearity and geometric nonlinearity were accounted for in the analysis.

*Shear force in flanges*

To investigate the shear force developed in the flanges, an elastic-perfectly plastic model was used for the steel in order to exclude the strain hardening effect of web steel on overstrength. The link model of Specimen L11 was monotonically loaded to an inelastic rotation of 0.15 rad, equal to its inelastic rotation capacity. The shear force in the link flanges was evaluated as the resultant shear force, with respect to the coordinate system fixed to the original configuration, acting on the flanges at mid-span of the link (using the "free body cut" command in ABAQUS). The total shear force in two flanges was nearly constant along the entire length of the link. Fig. 10(a) indicates that the shear force in the flanges for the link model increases along with an increase in link inelastic rotation. At 0.15 rad rotation, the flanges can develop a shear force equal to 17% of the plastic shear strength.

After the web is fully yielded in shear under a large inelastic rotation, it loses the restraint to the bending of flanges and stiffeners. At this stage, the link can be regarded as a virtual “frame” consisting of the flanges and stiffeners, plus filled panels that are yielded in shear, as shown in Fig. 10(b). The strength of the virtual “frame” is determined by a plastic collapse mechanism with hinges at flange ends and stiffener ends. The secondary moment of flanges leads to shear force developed in flanges. This implies that links with a larger flange area can develop a larger shear strength, which is consistent with the findings in past research that built-up steel shear links with heavy flanges exhibit high overstrength (McDaniel et al. 2003; Richards 2004). Moreover, the FE analysis indicates that, at a large inelastic rotation, secondary axial tensile force is produced in the flanges at the mid-span of the link. The component of the secondary axial force provides another source of shear contribution of the flanges.

A series of FE models were extrapolated from the reference model for Specimen L11. The sectional geometry of all models corresponded to the dimensions of Specimen L11, while a variety of link lengths was considered to investigate the effect of length ratio. Note that the spacing of intermediate web stiffeners for all models was taken as 220 mm. Fig. 11 shows the additional shear strength beyond $V_p$ taken at 0.15 rad inelastic rotation, which in these models, can be attributed to the flanges. For the range of link length examined in the figure, the contribution of the flanges increases along with a decrease of the link length ratio. For the hybrid link specimens in the test which had a length ratio of 0.58 through 0.97, and where the yield stress was 40% higher in the flanges than in the web, the flanges can increase the link strength beyond the plastic shear strength by 15 to 20%.

*Cyclic hardening of web steel*

Kasai et al. (2004) tested short steel panels with very small width-to-thickness ratio, where the steel panels developed a shear angle of 1.2 rad under monotonic shear loading and 0.15 rad under cyclic shear loading. They observed hardening continued to very large shear angles reaching 2.6 to 3.0 times the yield strength under monotonic shear loading and exceeding 2 times the yield strength under cyclic shear loading. Based on such findings and the result that the very short link specimens in this study exhibited much larger inelastic rotation than those reported in earlier shear link specimens, the large shear strains developed in the web was suspected to be a major cause of the larger than expected overstrength factor.

To quantify the cyclic hardening effect of web steel, a constitutive model that combines both kinematic and isotropic hardening was adopted to simulate plasticity of the steel in finite element analysis. The parameters of this hardening model were determined by the cyclic coupon test data in Dusicka et al. (2007) for LY225 steel and in Shi et al. (2011) for Q235 steel. In these coupon tests, the maximum stress developed by the coupons were 1.8 times the yield strength established from monotonic tension tests. The hysteresis curve of shear force versus link rotation obtained by FE analysis was compared with the test data, an example of which is shown in Fig. 12 for Specimen L11. The FE analysis results correlated well with the test results. The FE analysis indicated that the cyclic hardening effect can increase the shear strength by approximately 75% for the LY225 web link and by 65% for the Q235 web link.

## Conclusions

In this paper, a total of twelve cyclic loading tests were conducted on shear links used for replaceable coupling beams. Hybrid sections were used with Q345 steel for the flanges and LY225 or Q325 steel for the web. The shear links were very short, with a length ratio, $e/(M_p/V_p)$, less than 1.0. Major findings from the study are summarized as follows:

(1). The overstrength factors of the very short shear links reached 1.9. Although this value is much greater than 1.5 assumed for EBF links in the AISC 341-10 provisions, the value agrees with the general trend of a large number of test data reported in the literature. Finite element analysis indicated that the shear force in the flanges is substantial due to the very short link length, and it can increase the shear strength by 15 to 20% beyond plastic shear strength. In addition, when the link develops inelastic rotations on the order of 0.15 rad, cyclic hardening of the web steel can increase the shear strength by another 65 to 75%. The two contributions combined might explain the large overstrength factor of 1.9.

(2). The very short shear links achieved very large inelastic rotation capacity of 0.14 rad, significantly larger than 0.08 rad assumed for EBF links in the AISC 341-10 provisions.

(3). The difference in web steel material, LY225 or Q235, had little influence on the overstrength factor of the shear links. However, using LY225 steel instead of Q235 steel for web increased the inelastic rotation of the links by 25% and the cumulative plastic rotation by 44%.

(4). The link specimens whose stiffener spacing followed the AISC 314-10 requirement exhibited stable hysteretic responses and developed a large inelastic deformation capacity of 0.13 to 0.17 rad. The specimens which violated the stiffener spacing limit by 50% were affected by web buckling and associated strength degradation, however, successfully completed the 0.08 rad inelastic rotation cycles as required for EBF links in the AISC 341-10 provisions.

(5). Axial elongation of the link specimens grew larger as the specimens underwent large inelastic shear deformation. Axial forces arising from axial restraint should be accounted for when using very short shear links in coupling beams.

In conclusion, the study demonstrated the promising seismic performance of the very short links. The success of the proposed replaceable steel coupling beams relies on connections between the link and normal beam segments that allows damaged links to be replaced in the presence of residue drifts expected after a severe earthquake event. Various types of specialized connections have been developed and large-scale tests of the wall pier-beam segment-shear link system have been conducted to examine the performance of the steel coupling beams and replaceability of the shear link. The results will be presented in a future paper.

**Acknowledgements**

The work presented in this paper was sponsored by the International Science & Technology Cooperation Program of China (Grant No. 2014DFA70950), Tsinghua University Initiative Scientific Research Program (Grant No. 2012THZ02-1), National Key Technology R&D

Program of China (No. 2012BAJ07B01), and National Natural Science Foundation of China (Grants No. 51261120377 and No. 91315310). The writers wish to express their sincere gratitude to the sponsors.

## References

ABAQUS Analysis User’s Manual. Version 6.10. (2009). ABAQUS Inc., Dassault Systèmes.

AISC (American Institute of Steel Construction). (2010). “Seismic provisions for structural steel buildings.” *ANSI/AISC 341-10*, Chicago.

Chao, S. H., Khandelwal, K., and El-Tawil, S. (2006). “Ductile web fracture initiation in steel shear links.” *J. Struct. Eng.*, 132(8): 1192-1200.

Christopoulos, C., and Montgomery, M. S. (2013). “Viscoelastic coupling dampers (VCDs) for enhanced wind and seismic performance of high-rise buildings.” *Earthq. Eng. Struct. D.*, 42(15):2217-2233.

Chung, H. S., Moon, B. W., Lee, S. K., Park, J. H., and Min, K. W. (2009). “Seismic performance of friction dampers using flexure of RC shear wall system.” *Struct. Design Tall Spec. Build.*, 18(7):807-822.

CMC (Ministry of Construction). (1997). “Specification of testing methods for earthquake resistant building.” *JGJ 101-96*, Beijing. (in Chinese).

CMC (Ministry of Construction). (2013). “Technical specification for seismic energy dissipation of buildings.” *JGJ 297-2013*, Beijing. (in Chinese).

Dusicka, P., Itani, A.M., and Buckle, G. (2007). “Cyclic response of plate steels under large inelastic strains.” *J. Constr. Steel. Res.*, 63:156–164.

Dusicka, P., Itani, A. M., and Buckle, I. G. (2010). "Cyclic behavior of shear links of various grades of plate steel." *J. Struct. Eng.*, 136(4): 370-378.

El-Tawil, S., Harries, K. A., Fortney, P. J., Shahrooz, B. M., and Kurama, Y. (2010). "Seismic design of hybrid coupled wall systems: State of the art." *J. Struct. Eng.*, 136(7): 755-769.

Engelhardt, M. D., and Popov, E. P. (1989). "Behavior of long links in eccentrically braced frames." *Rep. No. UCB/EERC-89/01*. Earthquake Engineering Research Center, University of California, Berkeley.

Fortney, P. J., Shahrooz, B. M., and Rassati, G. A. (2007). "Large-scale testing of a replaceable steel coupling beam." *J. Struct. Eng.*, 133(12):1801-1807.

Hjelmstad, K. D., and Popov, E. P. (1983). "Seismic behavior of active beam link in eccentrically braced frames." *Rep. No. UCB/EERC-83/15*, Earthquake Engineering Research Center, University of California, Berkeley.

Itani, A. M. (2002). "Cyclic behavior of shear links and tower shaft assembly of San Francisco-Oakland Bay Bridge Tower." *Rep. No. CCEER 02-06*, Center for Civil Engineering Earthquake Research, University of Nevada at Reno, Reno.

Ji, X., Ma, Q., Wang, Y., and Qian, J. (2014). "Cyclic tests of replaceable shear links in steel coupling beams." *J. Build. Struct.*, 35(6):001-011 (in Chinese).

Kasai, K., and Popov, E. P. (1986). "A study of seismically resistant eccentrically braced frames." *Rep. No. UCB/EERC-86/01*, Earthquake Engineering Research Center, University of California, Berkeley.

Kasai, K., Ooki, Y., Suriyamongkol, P., and Xu, Y. (2004). “Fundamental study on inelastic behavior and low-cycle fatigue of a thick shear panel fabricated without welding.” *J. Struct. Constr. Eng.*,, 69(586):195-202 (in Japanese).

Malley, J. O., and Popov, E. P. (1984). “Shear links in eccentrically braced frames.” *J. Struct. Div.*, 110(9):2275-2295.

Mansour, N., Christopoulos, C., and Tremblay, R. (2011). “Experimental validation of replaceable shear links for eccentrically braced steel frames.” *J. Struct. Eng.*, 137(10):1141-1152.

McDaniel, C. C., Uang, C. M., and Seible, F. (2003). “Cyclic testing of built-up steel shear links for the new Bay Bridge.” *J. Struct. Eng.*, 129(6), 801-809.

Okazaki, T., Arce, G., Ryu, H. C., and Engelhardt, M. D. (2005). “Experimental study of local buckling, overstrength, and fracture of links in eccentrically braced frames.” *J. Struct. Eng.*, 131(10): 1526-1535.

Okazaki, T., and Engelhardt, M. D. (2007). “Cyclic loading behavior of EBF links constructed of ASTM A992 steel.” *J. Constr. Steel. Res.*, 63(6):751–765.

Okazaki, T., Engelhardt, M. D., Drolias, A., Schell, E., Hong, J. K., and Uang, C. M. (2009). “Experimental investigation of link-to-column connections in eccentrically braced frames.” *J. Constr. Steel. Res.*, 65(7):1401-1412.

Popov, E. P., and Engelhardt, M. D. (1988). “Seismic eccentrically braced frames.” *J. Constr. Steel. Res.*, 10: 321–354.

Ramadan, T., and Ghobarah, A. (1995). “Behavior of bolted link-column joints in eccentrically braced frames." *Can. J. Civil. Eng.*, 22(4):745-754.

Richards, P. W. (2004). "Cyclic stability and capacity design of steel eccentrically braced frames." Ph. D. dissertation. University of California, San Diego.

Ricles, J. M., Popov, E. P. (1986). "Experiments on eccentrically braced frames with composite floors." *Rep. No.UCB/EERC-87/06*, Earthquake Engineering Research Center, University of California, Berkeley.

Shi, Y., Wang, M., and Wang, Y. (2011). "Experimental and constitutive model study of structural steel under cyclic loading." *J. Constr. Steel. Res.*, 67(8): 1185-1197.

Teshigawara, M., Kato, M., Sugaya, K. and Matsushima, Y. (1998), "Energy Absorption Mechanism and the Fluctuation of shear Force in the Coupled shear Walls," Structural Engineering World Wide 1998 - Proceedings, Paper No. T-186-5.

**Table 1.** Material properties for steel

| Steel Type | Plate | Thickness $t$ (mm) | Yield strength $f_y$ (MPa) | Ultimate strength $f_u$ (MPa) | $f_u/f_y$ | Elongation (%) |
|---|---|---|---|---|---|---|
| Q345 | Flange | 14 | 319 | 479 | 1.50 | 41.9 |
| LY225 | Web | 10 | 228 | 330 | 1.45 | 54.0 |
| Q235 | Web | 10 | 273 | 416 | 1.52 | 44.4 |
| Q235 | Stiffener | 10 | 281 | 432 | 1.54 | 43.1 |

**Table 2.** Test variables of the specimens

| Specimen No. | Web steel | Length ratio | | Stiffener configuration | | Loading Protocol |
|---|---|---|---|---|---|---|
| | | *e* (mm) | $e/(M_p/V_p)$ | One side or both sides of web | Spacing (mm) | |
| L11C | | 660 | 0.87 | Both | 220 | JGJ 101-96 |
| L11D | | 660 | 0.87 | Both | 220 | JGJ 297-2013 |
| L11 | | 660 | 0.87 | Both | 220 | AISC 341-10 |
| L12 | LY225 | 660 | 0.87 | One | 220 | AISC 341-10 |
| L13 | | 660 | 0.87 | Both | 330 | AISC 341-10 |
| L21 | | 440 | 0.58 | Both | 220 | AISC 341-10 |
| L22 | | 440 | 0.58 | One | 220 | AISC 341-10 |
| Q11 | | 660 | 0.97 | Both | 220 | AISC 341-10 |
| Q12 | | 660 | 0.97 | One | 220 | AISC 341-10 |
| Q13 | Q235 | 660 | 0.97 | Both | 330 | AISC 341-10 |
| Q21 | | 440 | 0.64 | Both | 220 | AISC 341-10 |
| Q22 | | 440 | 0.64 | One | 220 | AISC 341-10 |

Note: the values of plastic strength ($V_p$) and plastic flexural strength ($M_p$) were based on the actual measured yield strength of the steel and actual measured dimensions.

**Table 3.** Damage and failure of specimens

| Specimen No. | Rotation at damage occurrence (rad) | | | | Failure mode |
|---|---|---|---|---|---|
| | Web buckling | Web fracture | Stiffener-to-flange weld fracture | Flange-to-end plate weld fracture | |
| L11C | 0.10 | 0.12 | 0.12 | 0.12 | Flange-to-end plate weld fracture |
| L11D | 0.08 (13th cycle) | — | — | 0.08 (14th cycle) | Flange-to-end plate weld fracture |
| L11 | 0.11 | 0.13 | 0.15 | 0.15 | Flange-to-end plate weld fracture |
| L12 | 0.08 | 0.11 | 0.09 | 0.19 | Web fracture |
| L13 | 0.07 | 0.13 | — | — | Web fracture |
| L21 | 0.11 | 0.11 | 0.13 | 0.15 | Flange-to-end plate weld fracture |
| L22 | 0.13 | 0.13 | — | 0.15 | Web fracture |
| Q11 | 0.09 | 0.11 | — | 0.13 | Flange-to-end plate weld fracture |
| Q12 | 0.09 | 0.11 | — | 0.13 | Flange-to-end plate weld fracture |
| Q13 | 0.07 | 0.11 | — | — | Web fracture |
| Q21 | 0.11 | 0.09 | 0.15 | 0.13 | Web fracture |
| Q22 | 0.09 | 0.09 | 0.11 | 0.13 | Web fracture |

**Table 4.** Shear strength and deformation capacity of specimens

| Specimen No. | Plastic shear strength $V_p$ (kN) | Maximum shear strength $V_{max}$ (kN) | Overstrength factor $\Omega$ | Inelastic rotation capacity $\gamma_p$ (rad) | Cumulative plastic rotation $\sum\gamma_p$ (rad) |
|---|---|---|---|---|---|
| L11C | 508 | 950 | 1.87 | 0.14 | 5.20 |
| L11D | 508 | 869 | 1.71 | 0.08 | 4.68 |
| L11 | 508 | 957 | 1.88 | 0.15 | 3.11 |
| L12 | 508 | 949 | 1.87 | 0.17 | 3.67 |
| L13 | 508 | 838 | 1.65 | 0.15 | 3.06 |
| L21 | 508 | 1037 | 2.04 | 0.15 | 3.13 |
| L22 | 508 | 1029 | 2.03 | 0.17 | 3.76 |
| Q11 | 593 | 1107 | 1.87 | 0.13 | 2.34 |
| Q12 | 593 | 1089 | 1.84 | 0.13 | 2.42 |
| Q13 | 593 | 970 | 1.64 | 0.11 | 1.95 |
| Q21 | 593 | 1180 | 1.99 | 0.13 | 2.45 |
| Q22 | 593 | 1130 | 1.91 | 0.13 | 2.47 |

464

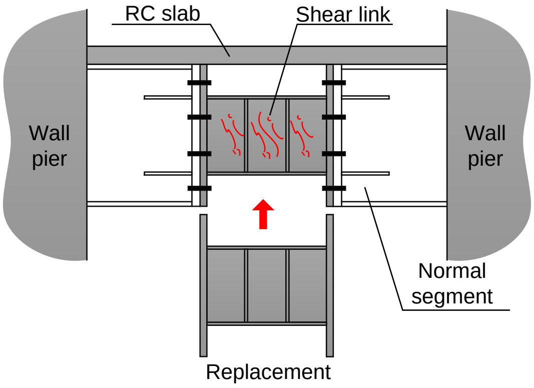


**Fig. 1.** Schematic drawing of replaceable steel coupling beam

465

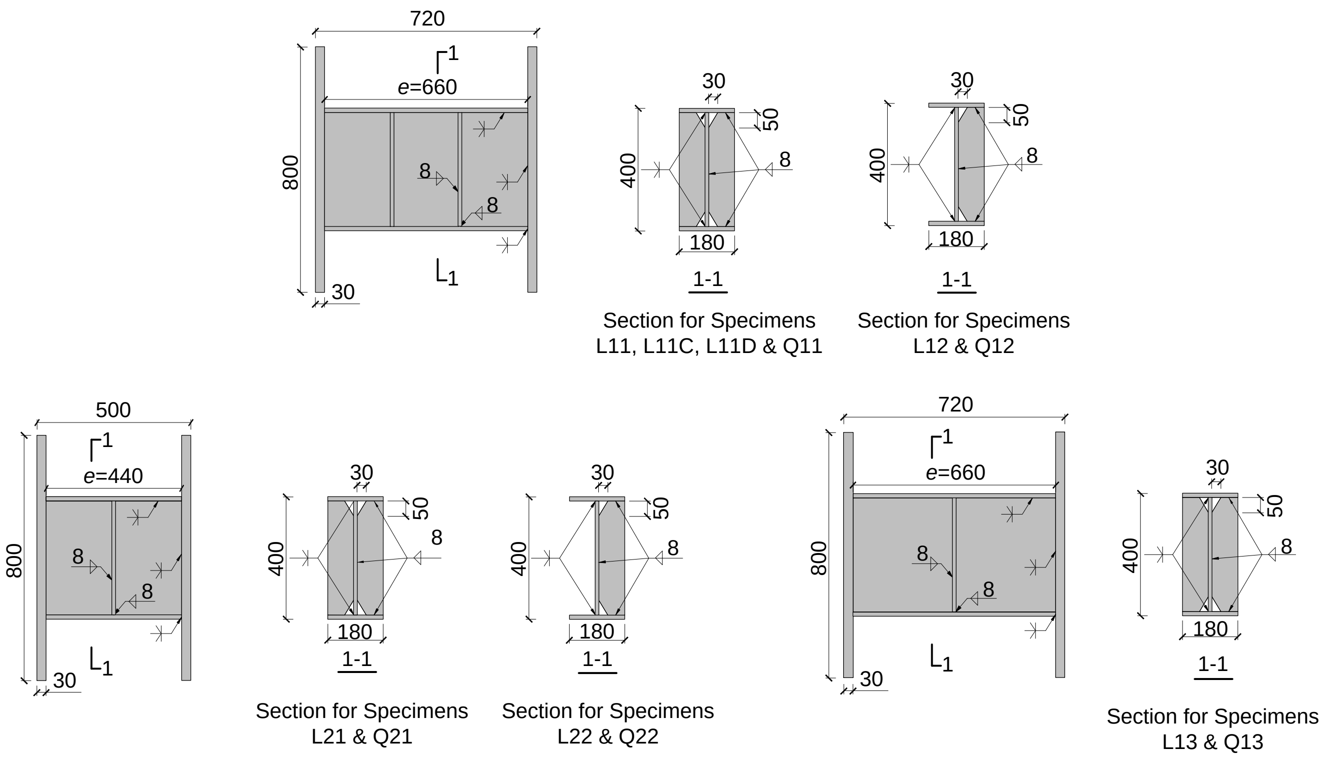


**Fig. 2.** Test specimens

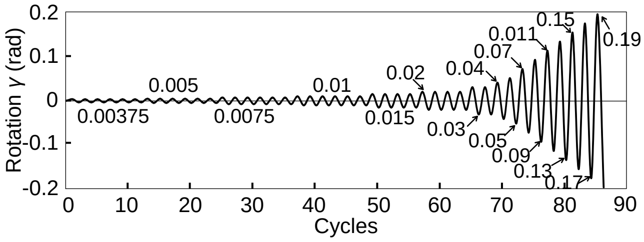


(a) AISC 341-10 loading protocol

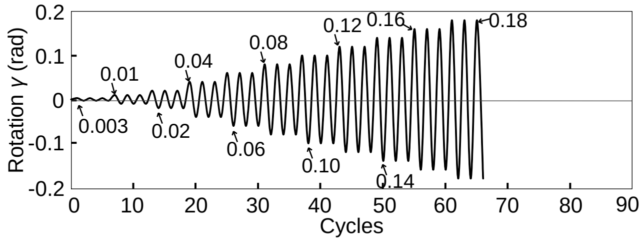


(b) JGJ 101-96 loading protocol

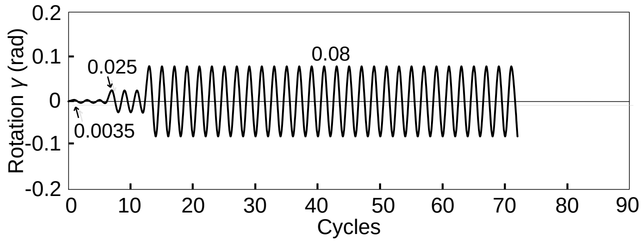


(c) JGJ 297-2013 loading protocol

**Fig. 3.** Loading protocols

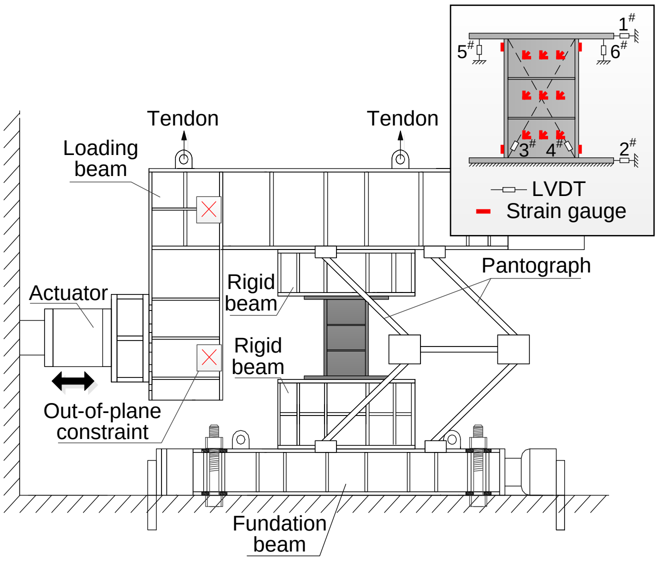


**Fig. 4.** Test setup and instrumentation

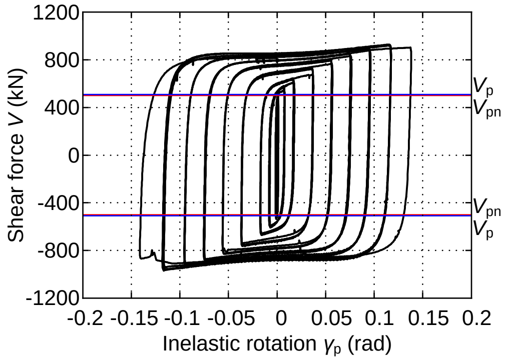


(a) L11C

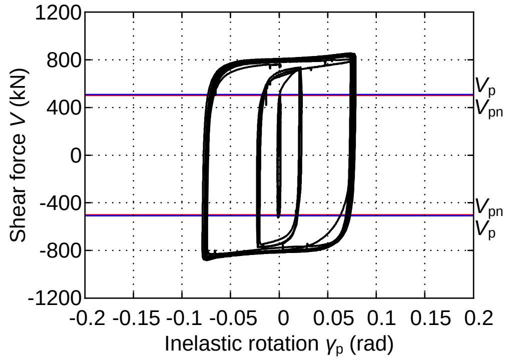


(b) L11D

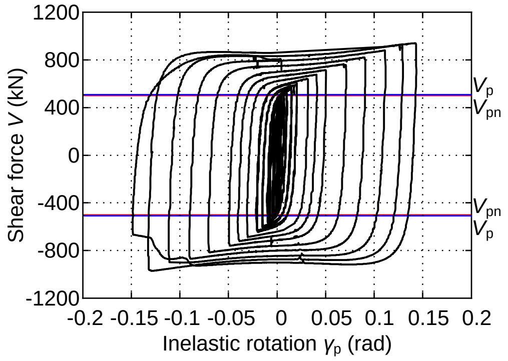


(c) L11

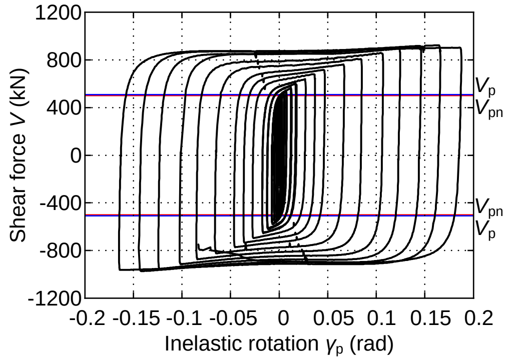


(d) L12

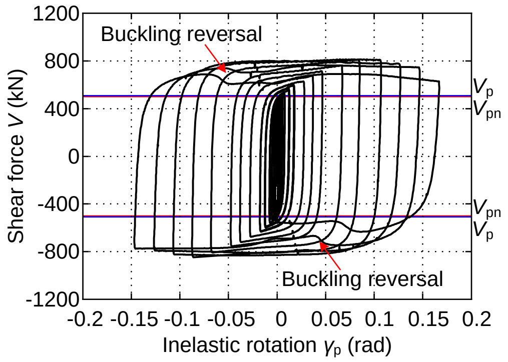


(e) L13

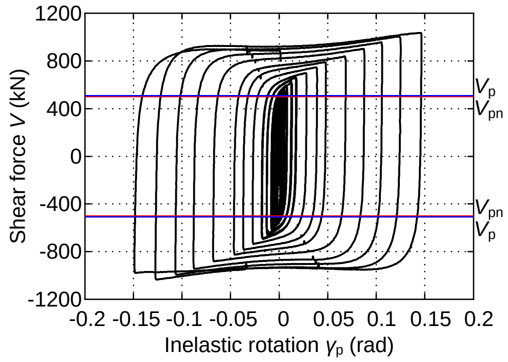


(f) L21

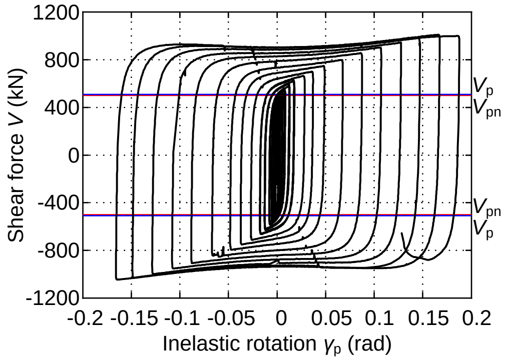


(g) L22

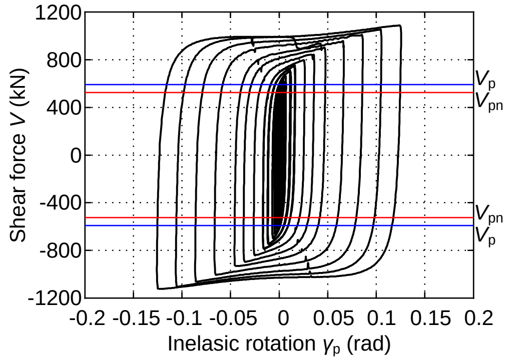


(h) Q11

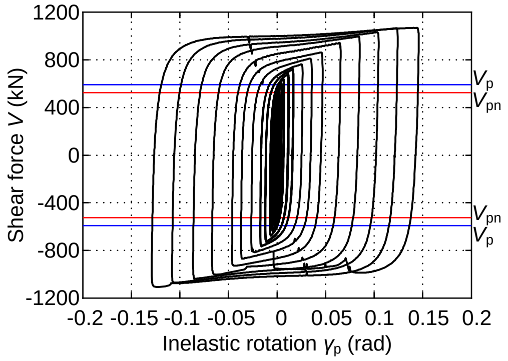


(i) Q12

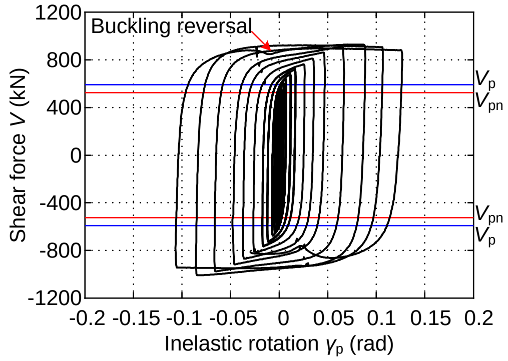


(j) Q13

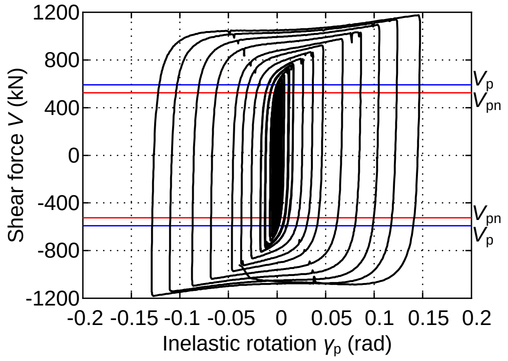


(k) Q21

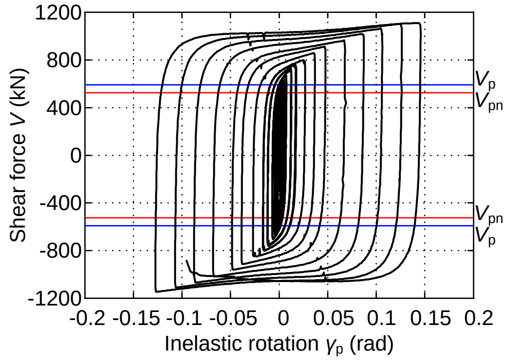


(l) Q22

**Fig. 5.** Hysteretic responses of specimens

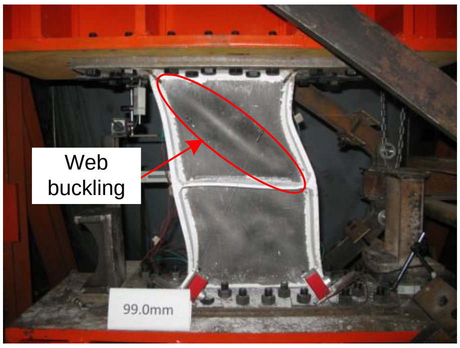


(a) Web buckling (Specimen L13)

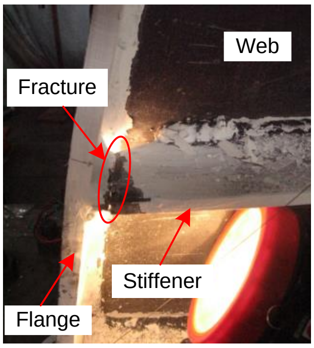


(b) Stiffener-to-flange weld fracture

(Specimen L22)

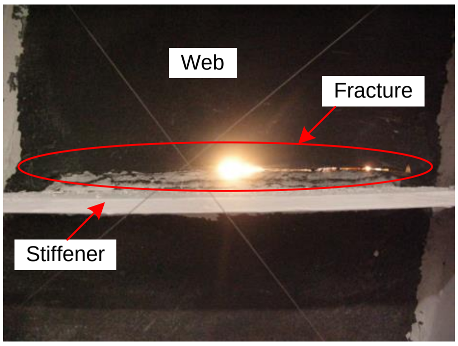


(c) Web fracture (Specimen L12)

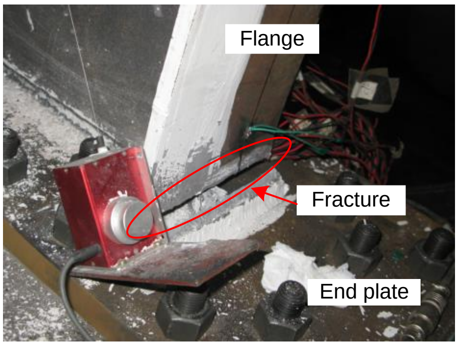


(d) Flange-to-end plate weld fracture

(Specimen Q12)

**Fig. 6.** Photographs of damage of specimens

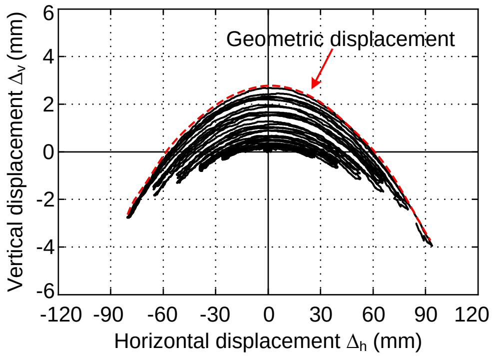


(a) Displacement orbit of Specimen L11C

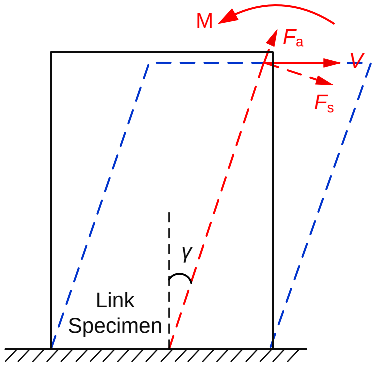


(b) Force decomposition at large inelastic rotation

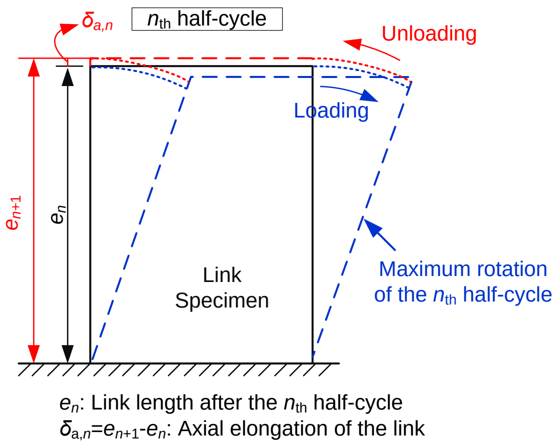


(c) Schematic view of displacement

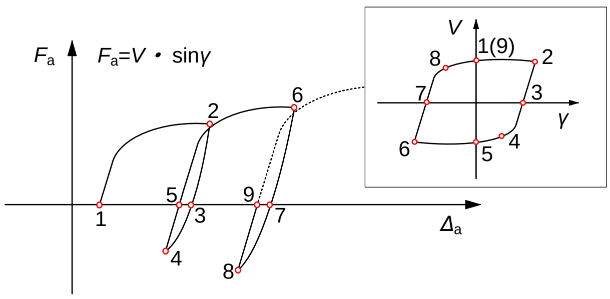


(d) Axial deformation developed in an inelastic loading cycle

**Fig. 7.** Axial deformation of shear link

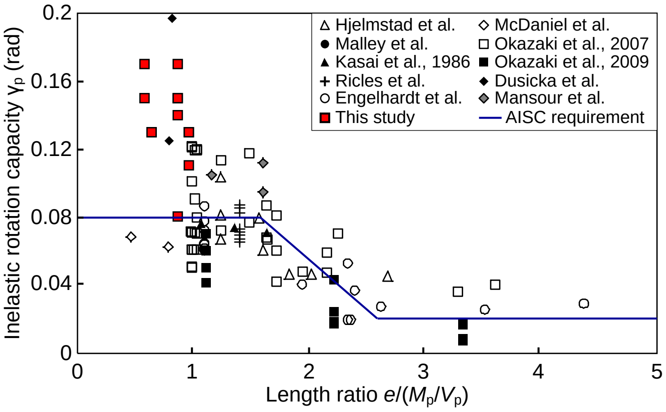


**Fig. 8.** Inelastic rotation capacity versus length ratio of shear links

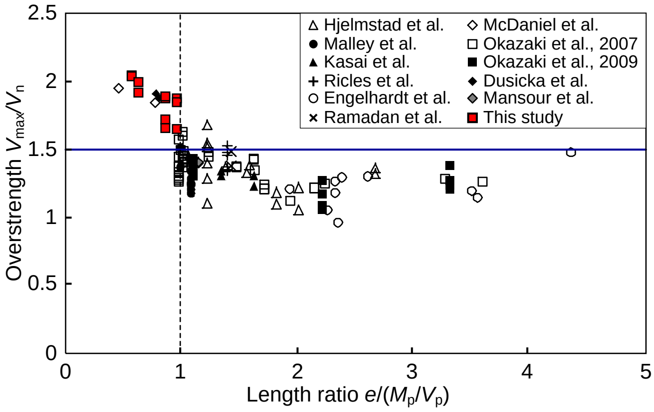


**Fig. 9.** Overstrength factors of link test data

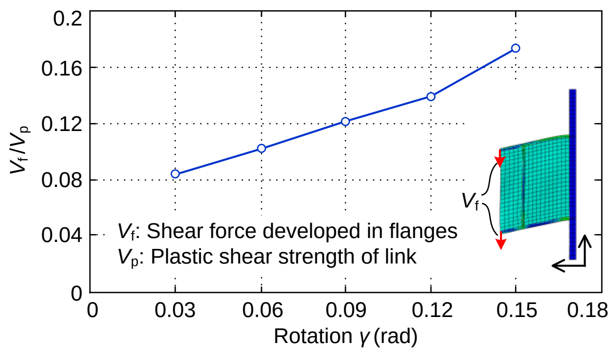


(a) Shear force in flanges (with respect to coordinate system fixed to original configuration)

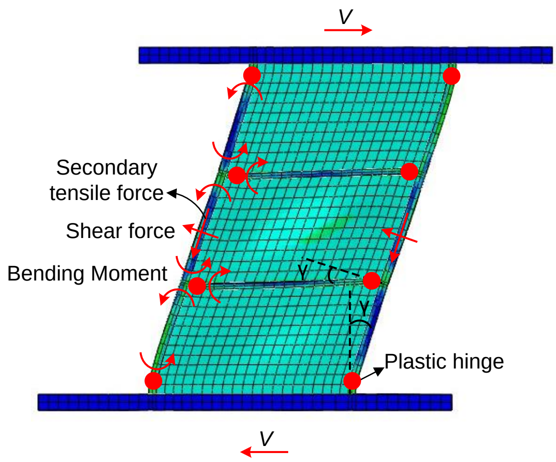


(b) Inner forces in flanges (with respect to coordinate system of deformed configuration)

**Fig. 10.** Forces developed in flanges of Specimen L11

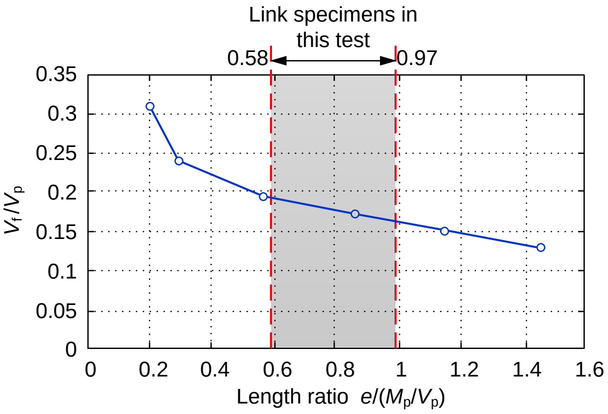


**Fig. 11.** Flange contribution on shear strength

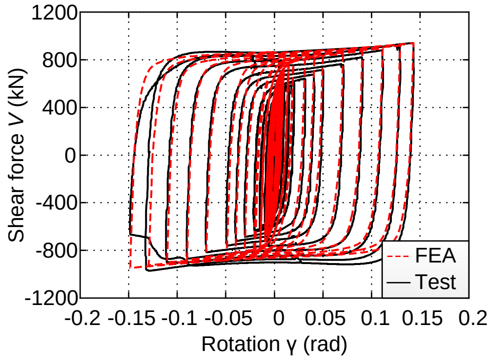


**Fig. 12.** Comparison between FE analysis result with test data for Specimen L11

**Fig. 1.** Schematic drawing of replaceable steel coupling beam

**Fig. 2.** Test specimens

**Fig. 3.** Loading protocols: (a) AISC 341-10 loading protocol; (b) JGJ 101-96 loading protocol; (c) JGJ 297-2013 loading protocol

**Fig. 4.** Test setup and instrumentation

**Fig. 5.** Hysteretic responses of specimens: (a) L11C; (b) L11D; (c) L11; (d) L12; (e) L13; (f) L21; (g) L22; (h) Q11; (i) Q12; (j) Q13; (k) Q21; (l) Q22

**Fig. 6.** Photographs of damage of specimens: (a) Web buckling (Specimen L13); (b) Stiffener-to-flange weld fracture (Specimen L22); (c) Web fracture (Specimen L12); (d) Flange-to-end plate weld fracture (Specimen Q12)

**Fig. 7.** Axial deformation of shear link: (a) Displacement orbit of Specimen L11C; (b) Force decomposition at large inelastic rotation; (c) Schematic view of displacement; (d) Axial deformation developed in an inelastic loading cycle

**Fig. 8.** Inelastic rotation capacity versus length ratio of shear links

**Fig. 9.** Overstrength factors of link test data

**Fig. 10.** Forces developed in flanges of Specimen L11: (a) Shear force in flanges (with respect to coordinate system fixed to original configuration); (b) Inner forces in flanges (with respect to coordinate system of deformed configuration)

**Fig. 11.** Flange contribution on shear strength

**Fig. 12.** Comparison between FE analysis result with test data for Specimen L11